



Full-Scale Field Performance of Geocell Reinforced-Fly Ash in the Subbase Course of Flexible Pavement

Rohan Deshmukh¹ · S. Patel¹ · J. T. Shahu²

Received: 5 March 2022 / Accepted: 1 May 2022 / Published online: 26 May 2022
© The Author(s), under exclusive licence to Springer Nature Switzerland AG 2022

Abstract

The full-scale field performance of geocell reinforced-fly ash as a subbase layer was evaluated by constructing three test sections in the widening part of the Sahol-Kim state highway (Surat, India). The in-situ modulus of the pavement layers was measured during construction by a light weight deflectometer (LWD) and post-construction by a falling weight deflectometer (FWD). During construction, a positive effect of geocell reinforced-fly ash was observed on composite in-situ modulus and quantified in terms of composite modulus improvement factor (CMIF). The CMIF value for the 100-mm high geocell reinforced-fly ash section was 1.19, and for the 150-mm high geocell reinforced-fly ash section was 1.39 against the granular control section. After construction, a positive effect of geocell reinforced-fly ash was observed on the average elastic modulus of the subbase layer and quantified in terms of modular ratio (MR). The MR values vary between 1.16 and 1.22 for a 100-mm high geocell reinforced-fly ash layer. The highest MR value of 1.30 was obtained by a 150-mm high geocell reinforced-fly ash layer. Furthermore, finite element analysis was carried out to determine service life ratio (SLR) against fatigue and rutting failure. The SLR value for geocell reinforced-fly ash sections against the granular control section was more than one for rutting and fatigue failure, confirming the suitability of geocell reinforced-fly ash in the subbase layer.

Keywords Fly ash · Geocell · Light weight deflectometer · Falling weight deflectometer · Composite modulus improvement factor · Modular ratio · Service life ratio

Introduction

Due to rapid socio-economic development, the construction of the road network has gained momentum in India. Construction of pavement, its maintenance, and a massive amount of construction material has required for widening purposes. Consequently, there is a scarcity of suitably graded conventional materials for pavement construction. The cost of extracting good-quality natural material is increasing. On the other hand, India generates more than 200 million tonnes of fly ash yearly [1]. It creates a substantial solid waste disposal problem and threatens the environment. The use of fly ash in bulk quantity in the pavement can resolve the issue of (i) waste disposal and (ii) scarcity of suitable

graded conventional material. The soaked California Bearing Ratio (CBR) values of fly ash vary from 9 to 12%. However, the minimum requirement of soaked CBR is 30% for subbase material as per the Indian Road Congress (IRC) [2]. Therefore, fly ash needs either stabilization or reinforcement before it can be utilized as a subbase layer.

Geocell reinforcement improves infill material strength by providing three-dimensional confinement and reduction in lateral spreading [3]. Like a slab action, a high bending stiffness value of the composite geocell mattress reduces induced stresses over subgrade [4]. The Geocell wall gives confinement to infill material and results in apparent cohesion to infill material [5]. The performance of geocell reinforcement was affected by the type of infill material. For example, load-carrying capacity increased by 13, 11, and 10 times for the aggregate, sand, and red soil infills compared to unreinforced soil bed [6]. Geocells improved the modulus of local marginal quality or recycled infill materials by an average of 2.75 times or more [7]. In another study [8], geocell reinforced fly ash was found to have seven times more load-carrying capacity than unreinforced fly ash beds. In yet

✉ Rohan Deshmukh
rohandeshmukh520@gmail.com

¹ Civil Engineering Department, S V National Institute of Technology, Surat, Gujarat, India

² Civil Engineering Department, Indian Institute of Technology, Delhi, India

another study, geocell reinforced fly ash bed exhibited less permanent deformations than unreinforced fly ash against static loading, showing two to three times improvement in the modulus [9]. Edil et al. (2006) [10] found substantial improvement in geocell-reinforced silty clay's resilient modulus but a slight improvement in geocell-reinforced gravel and sand through repeated load tests. In a field study, a geocell reinforced sand bed was found to have a higher rutting resistance under accelerated pavement testing (APT) facility compared to an unreinforced sand bed [11]. Al-qadi and Hughes [12] performed a falling weight deflectometer (FWD) test on geocell reinforced pavements and reported that the resilient modulus of 100-mm-high geocell reinforced aggregate was approximately two times compared to unreinforced aggregate.

Quality control by measuring the in-situ modulus of the granular layer has been successfully achieved by LWD testing [13, 14]. In a field study by Deshmukh et al. [15], the effect of geosynthetic reinforcements and their properties on the field modulus of the unpaved road was successfully evaluated using LWD.

Although several laboratory and field studies have been reported regarding the benefits of geocell reinforcement, studies where fly ash is used as fill material in the geocells,

are lacking which gave impetus to evaluate the field performance of the geocell reinforced-fly ash layer used as sub-base layer of flexible pavement. Three test sections were constructed (refer Table 1), and their in-situ performance was evaluated using light weight deflectometer (LWD) and falling weight deflectometer (FWD) testing during and after construction, respectively. The two geocell of different heights (i.e., 100 and 150 mm) were used in the test sections to assess the effect of geocell height on an in-situ modulus.

Field Study

Three test sections have been constructed in the widening part of the Sahol-Kim state highway in the Surat region of Gujarat, India. Two of these sections were built using geocell reinforcement with fly ash in the subbase layer, and one section was a conventional section with granular material for comparison. A cross-section with geocell reinforced-fly ash as a subbase layer is shown in Fig. 1a and a cross-section of the conventional unreinforced test section is shown in Fig. 1b.

Table 1 Details of test sections

Section number	Geosynthetic used	Subbase type	Geosynthetic location	Nomenclature of section	Total length (m)
S-1	Geocell 100 mm height	Fly ash	Bottom of subbase layer	GCE-100-FA-S	50
S-2	Geocell 150 mm height	Fly ash	Bottom of subbase layer	GCE-150-FA-S	50
S-3	Control section	GSB	–	CS	45

GCE Geocell, *FA* Fly ash, *CS* Control section, *GSB* Granular subbase

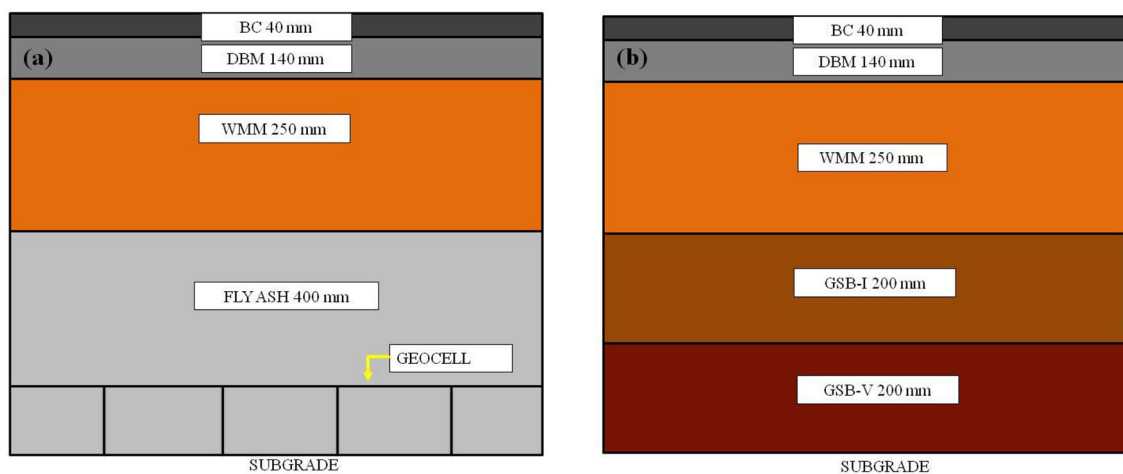


Fig. 1 A typical cross-section of the **a** geocell reinforced-fly ash test section and **b** unreinforced granular control test section

Materials

Extensive laboratory tests were done on the subgrade soil, granular base, subbase, and fly ash. The results of the testing are illustrated in the following section.

Subgrade Soil

Subgrade soil samples were collected from the test locations and tested for liquid limit (varied from 25.4 to 27.3%), plastic limit (varied from 5.02 to 6.53%), and plasticity index (varied from 19.51 to 21.98%). The subgrade soil had 40–45% clay, 30–35% silt, and 25–30% sand. The subgrade soil was categorized as low compressible clay as per the American Society for Testing and Materials (ASTM) D248-17 [16].

Granular Base and Sub Base

The Wet Mix Macadam (WMM) was used as the base layer in all the three-test section (S-1 to S-3), and the Granular Subbase (GSB) was used as the subbase layer only in the section S-3. Ministry of Road Transport and Highway (MoRTH) [17] specification was used to select WMM and GSB material grading. In the case of section S-3, the total 400-mm subbase layer contains two different grades of GSB, the bottom 200 mm was GSB-V, and the top 200 mm was GSB-I (Fig. 1b). The maximum dry unit weight values were 18.82, 19.80, and 22.26 kN/m³, and optimum moisture content (OMC) values were 5%, 3%, and 5.93% for GSB-V, GSB-I, and WMM, respectively. The D_{\max} (maximum particle size) was 74, 70, and 50 mm, and D_{50} (particle size corresponding to 50% finer in the particle size distribution) was 15, 14, and 12 mm for GSB-V, GSB-I, and WMM.

Fly Ash

In two sections (S-1 and S-2), fly ash was used as an infill material in geocell as a subbase layer. The optimum moisture content (OMC) and maximum dry density (MDD) of fly ash were found to be 21.66% and 13.33 kN/m³, respectively, as per Indian Standard (IS) 2720 (Part 7) [18]. Unconfined compressive strength of fly ash on the 7th and 28th day of curing was determined to find unconsolidated- undrained shear strength. Unconfined compressive strength of fly ash on the 7th and the 28th day was 0.69 MPa, and 0.85 MPa, respectively, and corresponding unconsolidated- undrained shear strength was 0.34 MPa and 0.42 MPa. The soaked CBR value for fly

ash was 11.4% as per IS 2720 (Part 16) [19]. The fly ash was ‘Class F’ type as per ASTM C618-17 [20].

Geocell

All the geocell’s mechanical, physical, and chemical properties are listed in Table 2. Geocell materials were provided free of cost by Maccaferri (India), along with the test results of geocell. Geocell in all the sections was selected as per the guidelines and requirements suggested by MORTH [17] section number 700.

Methodology

A total of three test sections were built to study the field performance of geocell reinforced-fly ash in the subbase layer (Table 1). In-situ LWD testing was conducted during construction over the base layer to determine the effect of ‘geocell reinforced-fly ash’ and ‘height of geocell’ on composite in-situ modulus (Fig. 2c). Test sections were completed in June 2019, then immediately, the Sahol-Kim state highway with its newly constructed widening lane was open for traffic. After that, the test sections’ built-in widening lane was undergone for FWD testing in August 2019 and February 2021 (Fig. 2d).

The terminologies used for test sections are self-explanatory and are given in Table 1. For example, GCE-100-FA-S indicates a section consist a 100-mm-high geocell with fly ash and geocell placed at the bottom of the subbase layer.

During construction, the performance of the geocell reinforced-fly ash test section was evaluated in terms of composite modulus improvement factor (CMIF) and determined using Eq. (1),

$$\text{CMIF} = \frac{E_{LWD(2)}}{E_{LWD(1)}} \quad (1)$$

where, $E_{LWD(2)}$ = Composite in-situ modulus (in MPa) from LWD test for geocell reinforced-fly ash sections (S-1, S-2), $E_{LWD(1)}$ = Composite in-situ modulus (in MPa) from LWD

Table 2 Properties of the geocell given by the manufacturer

Properties	Unit	Specified value	Average value
Polymer density	kg/m ³	935–965	959
Carbon black content	%	Min. 2.00	2.24
Nominal sheet thickness (post texturing)	mm	Min. 1.50	1.52
Weld spacing	mm	356	356
Cell height	mm	100 and 150	100 and 150
Expanded cell area	mm ³	289,000	290,000
Seam peel strength	kN	2.13	4.34
Tensile strength	kN/m	Min. 16	21.67



Fig. 2 a Installation of geocell, b filling of geocell, c LWD testing over the base layer, and d FWD testing over bituminous layer

test for conventional control section (S-3). The performance of geocell reinforced-fly ash sections (S-1, S-2) was checked against the conventional control section (S-3). LWD test was performed on the top of the 250 mm base layer (WMM) and hence recorded reading was composite in-situ modulus (E_{LWD}) of subgrade, subbase, and base layer.

After construction, the performance of the geocell reinforced-fly ash test section was evaluated in terms of modular ratio (MR) and calculated using Eq. (2),

$$MR = \frac{\text{Average modulus of geocell reinforced – fly ash layer}}{\text{Average modulus of granular subbase layer}} \quad (2)$$

The average modulus of the geocell reinforced-fly ash layer and the average modulus of the granular subbase layer was measured using FWD testing.

Geocell Reinforced-Fly Ash and Conventional Control Test Sections

The use of large amounts of fly ash in the pavement can address two challenges at once: waste disposal and the protection of a natural resource, namely aggregates [21]. Section S-1 and S-2 were constructed with a 400 mm fly ash layer in the subbase layer reinforced with 100 and 150 mm high geocell, respectively, placed at the bottom of the fly ash layer (Table 1; Fig. 1a). The base layer was 250-mm WMM, and the top surface layer was 140-mm dense bituminous macadam (DBM) and 40 mm bituminous concrete (BC).

The test section S-3 was constructed with conventional pavement materials, i.e., 400 mm GSB and 250 mm WMM, to compare the geocell reinforced-fly ash test sections (Table 1; Fig. 1b). The top surface layer was built with 140-mm dense bituminous macadam (DBM) and 40-mm bituminous concrete (BC).

Construction and Field Testing

The test sections were designed for traffic intensity of 30 million standard axles (MSA) and subgrade CBR of 3% as per IRC-37: 2012 [22]. The top width of the widening part (test section) was 4.90 m, and the bottom width was 5.05 m.

Installation of Geocell

Each geocell layer was 6.5 m in length and 2.59 m in width. The stretching of the geocell was done with anchoring at the corner and at regular intervals along the length. The connection with the next geocell layer was made using binding steel wire. An installed geocell layer in the subbase layer is shown in Fig. 2a and b. Extra care was taken during the filling of the geocell pocket to avoid damage to the geocell walls. Rolling was allowed only after infilling and placing a minimum 150-mm fly ash layer over the geocell.

Quality Control and Field Testing

During the construction of test sections, quality control over a specified degree of compaction was achieved by the sand replacement method as per IS 2720 (Part 28) [23]. The field dry density of fly ash and granular material was found in the range of 12.55 to 13.63 kN/m³ and 21.96 to 22.45 kN/m³, respectively, and optimum moisture content in the range of 18.7–22.3% and 2.00–5.20%, respectively. The in-situ compaction of the WMM varied from 97.6–99.2%.

Dynamic Cone Penetration Test (DCPT)

A dynamic cone penetrometer (DCPT) was performed in accordance with ASTM D6951 [24]. A total 400-mm sub-base layer was placed in two layers of 200 mm. DCPT test was conducted over the first layer of a 200-mm-thick Fly ash and GSB layer. The location of the DCPT tests is shown in Fig. 3. CBR values were determined using Eq. (3) given in ASTM D6951 [24],

$$CBR = \frac{292}{(DCPI)^{1.12}} \tag{3}$$

where DCPI Dynamic cone penetration index and CBR California bearing ratio.

Light Weight Deflectometer (LWD)

LWD is a handheld falling weight deflectometer that is used to measure the in-situ modulus of soil and granular layer. LWD test is suitable for quality assurance of subgrade, sub-base, and thin, flexible pavement constructions to check compliance with requirements. The LWD used in this study is shown in Fig. 4. The LWD weighed approximately 22 kg with a standard drop weight of 10 kg, making it highly

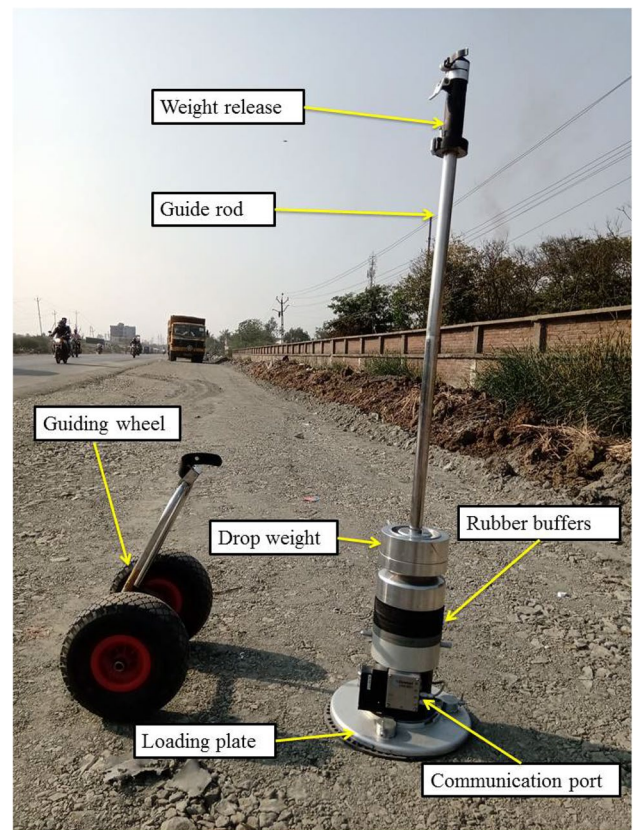
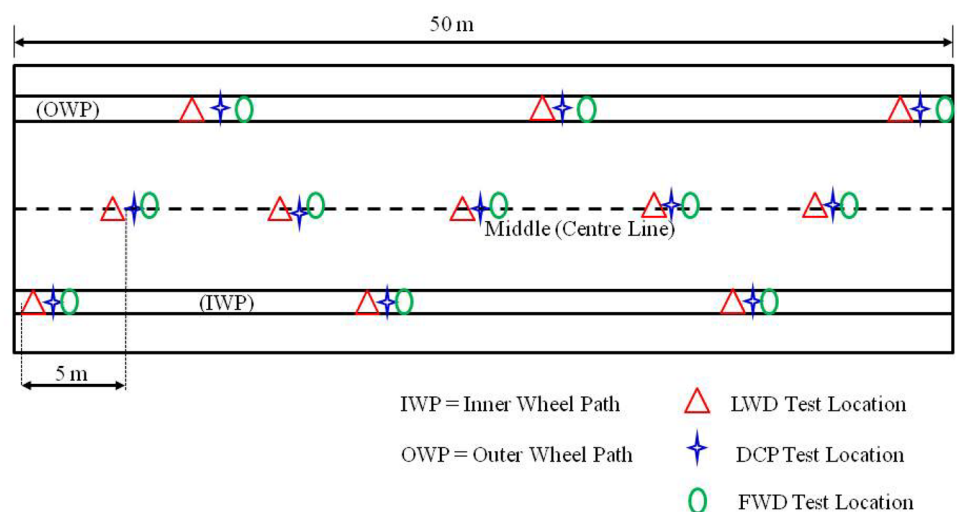


Fig. 4 Light weight deflectometer (LWD)

portable and easy to carry on a construction site. With an additional optional 10 kg weight, the LWD could produce up to 15 kN peak loads.

The LWD tests were conducted in accordance with ASTM E2583 [25]. The program uses a shape factor and Poisson's ratio as input parameters for calculating the modulus according to Eq. (4) [26],

Fig. 3 Location of quality control and field testing



$$E_{LWD} = \frac{f(1 - \nu^2) \cdot \sigma \cdot r}{\delta} \quad (4)$$

where E_{LWD} is the composite in-situ modulus, f is the shape factor, ν is Poisson's ratio, σ is applied stress, r is the radius of the loading plate, and δ is surface deflection.

The location of LWD tests is shown in Fig. 3. Testing was carried out on the centreline, outer wheel path (OWP), and inner wheel path (IWP). A load of 15 kg was used during the testing with the maximum drop height of 680 mm, which produces an impulse load of 9.3–10 kN and average stress of 130–143 kPa on the top of the base layer.

Falling Weight Deflectometer (FWD)

A Falling Weight Deflectometer (FWD) is an impulse-loading device (Fig. 5c). The weights fall with a pre-determined height on the loading plate to produce desired pressure on the pavement (Fig. 5a and b). The pressure produces deflections in the pavement, which are captured by a series of geophone sensors rested on the pavement surface during the impact of loading (Fig. 5b). The peak load and peak deflections are recorded by geophone sensors placed at radial locations.

Test locations were selected so that it covers the entire area of the test section to get a clear picture of the modulus values of a particular test section (Fig. 3). Three drops were applied at every test location; the first drop represents the seating load, the second drop represents 40 kN load, and the third drop means 55 kN load. Loads were adjusted by dropping the height of the whole load assembly of FWD. The FWD tests were performed as per IRC-115: 2014 [27].

Performance evaluation of test sections was carried out by conducting periodic FWD testing (in August 2019 and February 2021) overall three test sections. Deflection data collected from FWD testing were processed in ELMOD-6 software to calculate the modulus values of each layer of the test section. Modulus values of pavement layers are the governing factor for the performance evaluation of test sections.

Results and Discussion

A series of DCP, LWD, and FWD testing was carried out on test sections to evaluate the performance of 'geocell reinforced-fly ash' as a subbase layer in the pavement. The results of DCP, LWD, and FWD tests are summarised and discussed below.

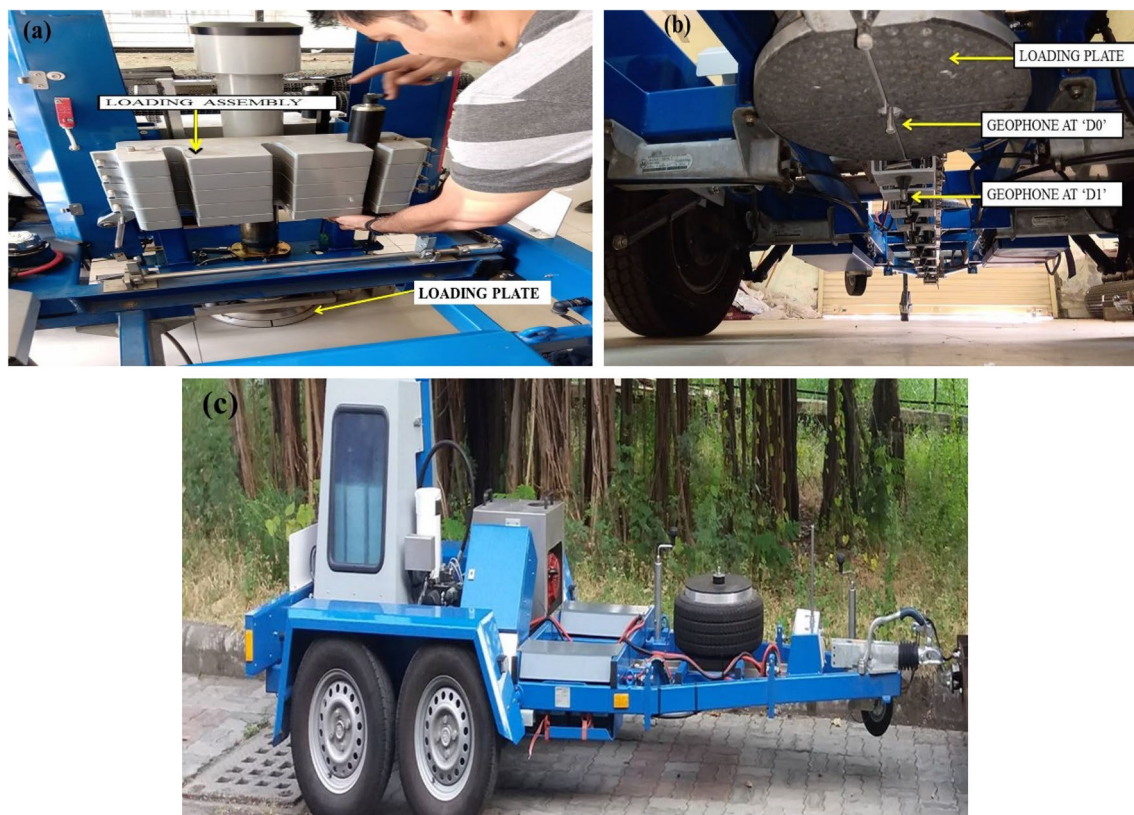


Fig. 5 a Loading assembly, b loading plate with geophone sensor, and c falling weight deflectometer (Model-Dynatest 8081)

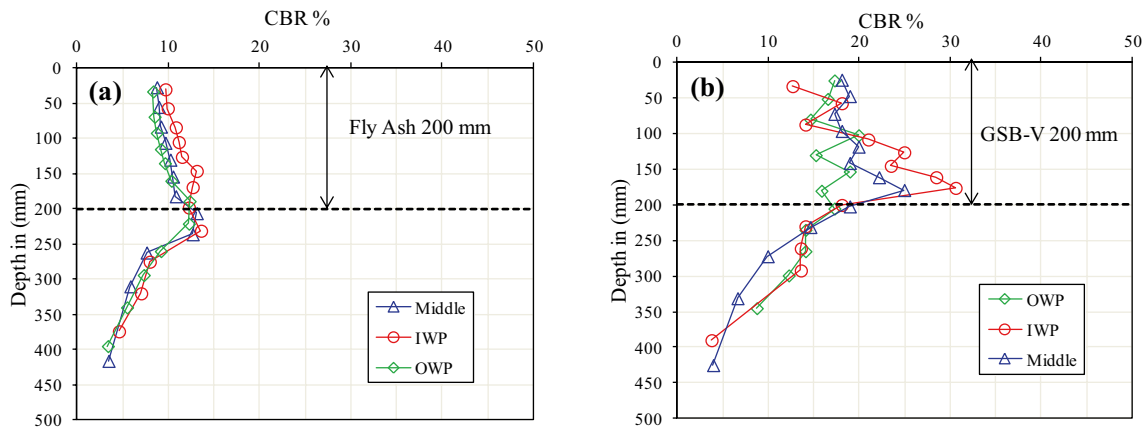


Fig. 6 CBR against penetration depth for section a S-1 and b S-3

Table 3 The composite elastic modulus for test sections in MPa from the LWD test

Section number	Location of LWD testing on	Test points	Maximum	Minimum	Median	COV (%)	Mean	Mean for section (E_{LWD})	CMIF
S-1	IWP	9	77.5	63.3	70.1	8.69	70.84	66.63	1.19
	Centre	9	71.5	61.2	67.9	4.39	66.95		
	OWP	9	66.9	59.5	62.3	3.63	62.08		
S-2	IWP	9	86	72.1	78.2	6.55	78.07	77.54	1.39
	Centre	9	90	68.6	75.2	10.19	77.01		
	OWP	9	88.1	66.2	74.1	11.65	75.94		
S-3	IWP	8	58.2	50.1	53.3	5.11	53.53	55.70	1
	Centre	8	58.1	52.3	57	3.27	56.36		
	OWP	8	59.3	53.4	58.1	3.93	57.21		

DCP tests

The results of DCP tests for sections S-1 and S-3 are given in Fig. 6a and b, respectively, in terms of CBR value against depth. Variations in CBR values for the top 200 mm are comparatively more minor, and values decrease abruptly. This assures the uniform thickness and compaction of the 200-mm fly ash and GSB layer.

LWD tests

The results of LWD testing for all the three test sections (S-1, S-2, and S-3) are given in Table 3. The test sections S-1 and S-2 were constructed with geocell-reinforced fly ash as a subbase layer with 100 and 150 mm geocell height. LWD testing was carried out on both the test sections S-1 and S-2 at 27 locations each. The maximum and minimum E_{LWD} value for 100 mm high geocell (section S-1) is 77.5 and 59.5 MPa, respectively, with a coefficient of variance (COV) of 3.63% to 8.69%. The average E_{LWD} for section S-1 with 100 mm high geocell is 66.63 MPa (Fig. 7). The maximum

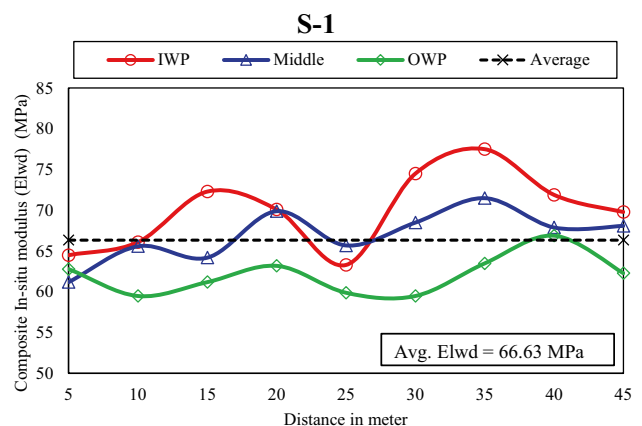


Fig. 7 E_{LWD} (MPa) values for 100 mm high geocell-reinforced fly ash section (S-1)

and minimum E_{LWD} value for 150 mm high geocell (section S-2) is 90 and 66.2 MPa, respectively, with COV of 6.55% to 11.65%. The average E_{LWD} for section S-2 with 150 mm high geocell is 77.54 MPa (Fig. 8).

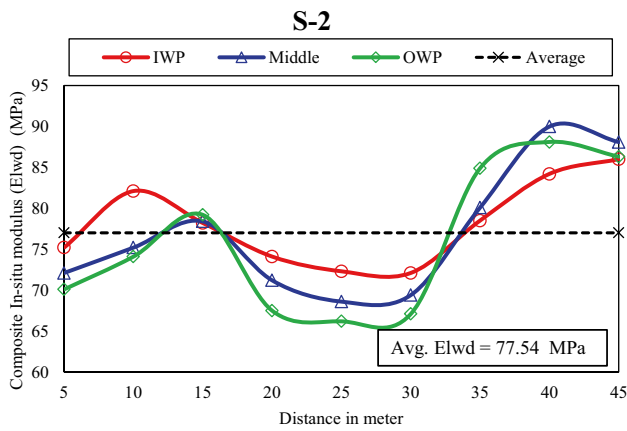


Fig. 8 E_{LWD} (MPa) values for 150 mm high geocell-reinforced fly ash section (S-2)

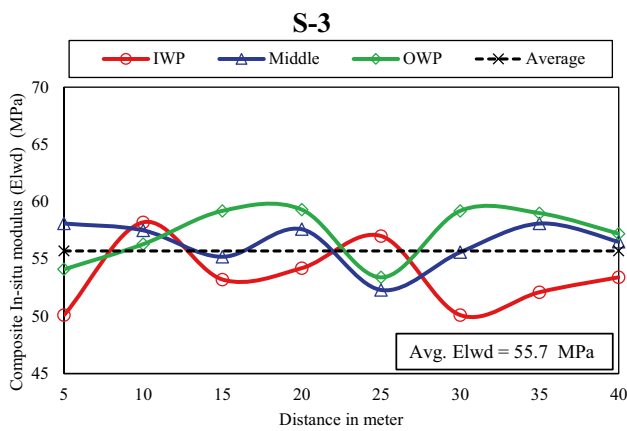


Fig. 9 E_{LWD} (MPa) values for granular control section (S-3)

The test section S-3 was constructed with a granular subbase layer. In 24 locations, LWD testing was carried out over section S-3. The maximum and minimum E_{LWD} value for section S-3 is 59.3 and 50.1 MPa, respectively,

with COV of 3.93% to 5.11%. The average E_{LWD} for section S-3 is 55.70 MPa (Fig. 9).

Composite Modulus Improvement Factor (CMIF)

The average E_{LWD} values for section, fly ash + 100 mm high geocell (S-1) and fly ash + 150 mm high geocell (S-2), are 66.63 and 77.54 MPa, respectively. These moduli were compared with the conventional granular control section's average E_{LWD} (55.70 MPa) (S-3). The CMIF values are calculated using Eq. 1. The CMIF value for the 100 mm high geocell-reinforced fly ash section (S-2) is 1.19 and for the 150-mm high geocell-reinforced fly ash section (S-3) is 1.39 (Table 3) against of granular control section (S-1). The inclusion of geocell reinforcement in the fly ash improves the CMIF value due to the three-dimensional confinement effect of geocell.

FWD tests

The results of FWD testing for all the three test sections (S-1, S-2, and S-3) are given in Table 4. Test sections were completed in June 2019; after that, test sections constructed in the widening lane were undergone for FWD testing in August 2019 (first testing) and February 2021 (second testing). Two FWD loads (40 kN and 55 kN) were used during each testing, and geophone sensors recorded deflections. To evaluate each layer's modulus value, recorded deflection data of individual test sections are then used in ELMOD 06 software for the back-calculation process. During each testing, FWD testing was carried out on a total of 27 points for each test section S-1 and S-2 and a total of 24 points for section S-1.

In Fig. 10, the average elastic modulus of the subbase layer for the FWD test load of 40 kN is shown for both testing periods. It is observed that with the time (from August 2019 to February 2021), the subbase layer's modulus values increase for the same FWD load (40 kN). Also, the elastic modulus of the geocell reinforced-fly ash subbase layer (S-1 and S-2) is more than the granular subbase layer (S-3) which

Table 4 Elastic modulus of sub-base layer in MPa from FWD test and modular ratio

Section	FWD testing in							
	August 2019				February 2021			
	FWD load-40 kN		FWD load-55 kN		FWD load-40 kN		FWD load-55 kN	
Elastic Modulus	Modular Ratio (MR)	Elastic Modulus	Modular Ratio (MR)	Elastic Modulus	Modular Ratio (MR)	Elastic Modulus	Modular Ratio (MR)	
S-1	69	1.16	71	1.16	77	1.18	81	1.22
S-2	75	1.27	79	1.29	84	1.29	86	1.30
S-3	59	1	61	1	65	1	66	1

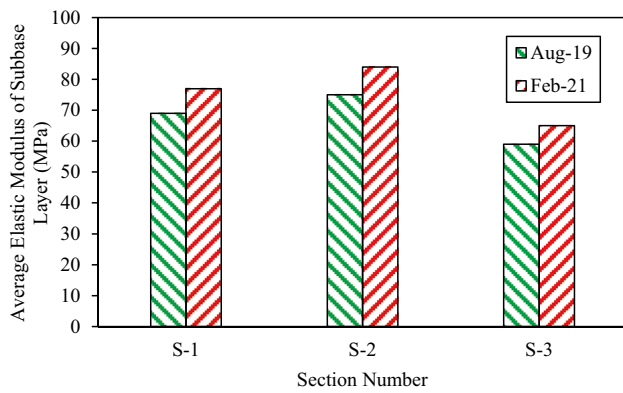


Fig. 10 Elastic modulus of sub-base layer (MPa) for FWD test load of 40 kN

confirms the suitability of the same in the subbase layer. In Fig. 11, the average elastic modulus of the subbase layer for the FWD test load of 40 kN and 55 kN is shown for the second testing (February 2021). It is observed that FWD loading has shown a slight positive effect on the elastic modulus value; it is mainly due to an increase in hoop stresses in the geocell wall with an increase in FWD loading.

Modular Ratio (MR)

The performance of the ‘geocell reinforced-fly ash’ layer is quantified in terms of modular ratio (MR). The MR values are calculated using Eq. (2) and presented in Table 4. The MR values were calculated for both the FWD load (44 kN and 55 kN) and the testing periods (August 2019 and February 2021). In each testing, the MR value of the ‘geocell reinforced-fly ash’ layer is greater than 1; it shows the suitability of ‘geocell reinforced-fly ash’ as a subbase layer in the pavement. The highest MR value of 1.30 is obtained by a 150 mm high geocell reinforced-fly ash layer during second FWD testing with 55 kN loading.

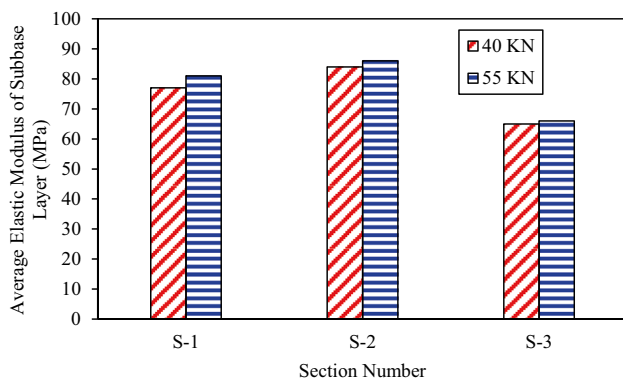


Fig. 11 Elastic modulus of sub-base layer (MPa) for second FWD testing (February 2021)

Finite Element Analysis

Finite element (FE) analyses were carried out to evaluate all three test sections' service life ratios (SLR). FE analyses were carried out using PLAXIS 2D for a five-layer flexible pavement system. The thickness for all the layers above the subgrade was determined as per IRC: 37–2012 [22] for 30 MSA traffic intensity and Subgrade CBR of 3%. The test sections were modeled as an axisymmetric solid, with all layers of 15-noded triangular elements. The boundary condition used and adopted fine mesh during modeling is shown in Fig. 12. Boundaries were assigned to the outer perimeter, axis of rotation and the bottom of the model. The axis of rotation and the outer perimeter were allowed to move vertically only whereas the bottom of the model was restricted for movement in both horizontal and vertical direction. As the pavement layers experience dynamic loading (Axle loads or FWD loads with loading frequency > 5 Hz) the corresponding strains are very low in magnitude as compared to the failure strain of the material. Therefore, it is assumed that the pavement layers will exhibit linear elastic behavior. Therefore, in PLAXIS linear elastic model was used to simulate pavement layers. Uniform stress of 575 kPa was applied over a circular area with a radius equal to 150 mm, representing a single-axle wheel load of 40 kN. The material properties used for finite element analysis are given in Table 5. The elastic modulus values for the subbase layer (GSB, FA + 100 mm GCE, and FA + 150 mm GCE) were taken as average in-situ modulus obtained during second FWD testing (February 2021) for both 40 and 55 kN loading (Refer Table 4). The elastic modulus for the base layer (WMM) was 135 MPa for all three sections, which was obtained for the unreinforced granular control section during the second FWD testing with a 40 kN load. The elastic modulus values for bituminous concrete (BC) and dense bituminous

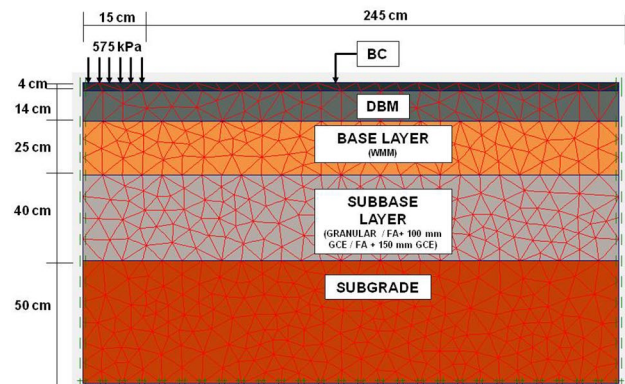


Fig. 12 Finite-element model of flexible pavement system using code PLAXIS

Table 5 Parameters used for the finite-element analysis of pavement

Parameter	3% CBR Subgrade	GSB	FA + 100 mm GCE	FA + 150 mm GCE	WMM	DBM	BC
E (MPa)	30	66 (55 kN), 65 (40 kN)	81 (55 kN), 77 (40 kN)	86 (55 kN), 84 (40 kN)	135	3000	3000
ν	0.35	0.35	0.35	0.35	0.35	0.35	0.35
γ (kN/m ³)	17.7	21.4	13.33	13.33	21.9	22.6	23.3

macadam (DBM) were taken from IRC: 37–2012 [22] for the viscous grade (VG)-40 (at a temperature of 35 °C). The elastic modulus (E) for subgrade of CBR 3% was determined as per Eq. (5), given in IRC: 37–2012.

$$E(\text{MPa}) = 10 \times \text{CBR} \tag{5}$$

Service Life Ration(SLR)

Finite element analysis was done to measure critical strains, namely, vertical compress strain (ϵ_v) and horizontal tensile strain (ϵ_t). In Figs. 13 and 14, compression strain (ϵ_v) and

tensile strain (ϵ_t) contours are shown for all three sections, respectively. Strain contours shown in Figs. 13 and 14 were found for the modulus value obtained for the subbase layer by FWD load of 55 kN (refer Table 5). Similarly, strain contours were also found for the modulus value obtained for the subbase layer by FWD load of 40 kN. Critical vertical compressive strain (ϵ_v) was measured at the top of subgrade and horizontal tensile strain (ϵ_t) was measured at the bottom of bituminous layer. Recorded critical strains for all the test sections are given in Table 6. The Eqs. (6) and (7) were used by Shahu et al. [28] and Chaudhary et al. [29] to determine the SLR of pavement against rutting and fatigue failure, respectively. The SLR of pavement against rutting failure is calculated by Eq. (6),

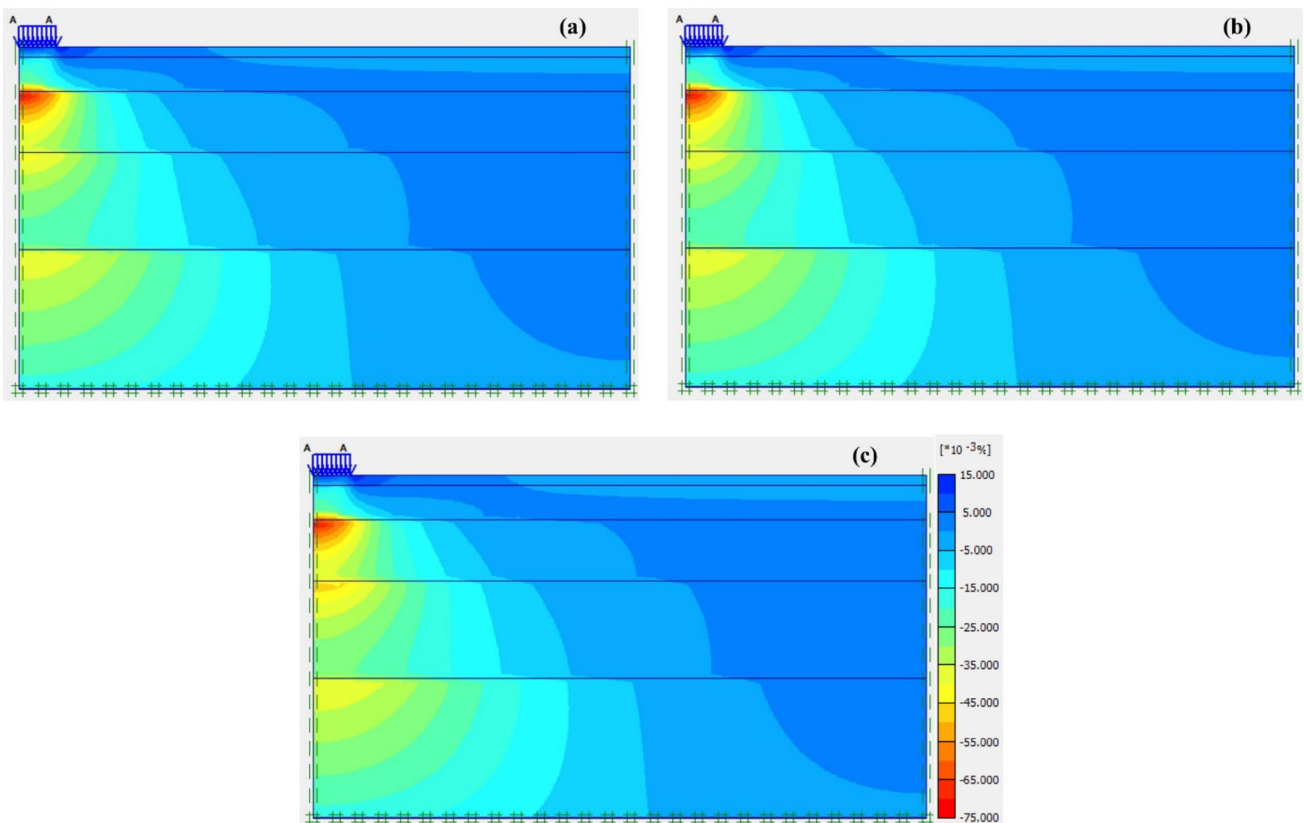


Fig. 13 Compression strain (ϵ_v) contours for section **a** S-1, **b** S-2, and **c** S-3

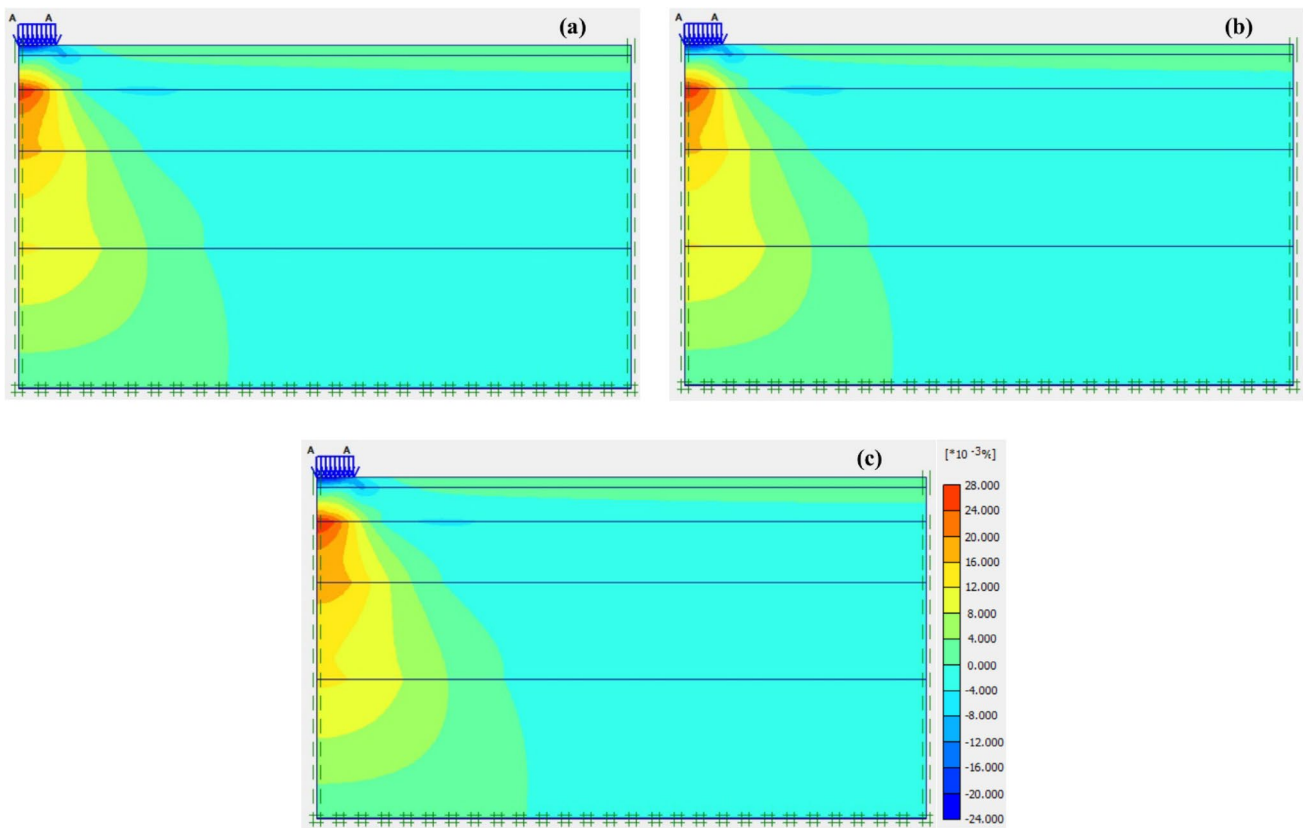


Fig. 14 Tensile strain (ϵ_t) contours for section a S-1, b S-2, and c S-3

Table 6 Service life ratio for all the test sections

Section Number	ϵ_t (micron)		ϵ_v (micron)		SLR (fatigue)		SLR (rutting)	
	40 kN	55 kN	40 kN	55 kN	40 kN	55 kN	40 kN	55 kN
S-1	216.4	215.5	419	418	1.04	1.06	1.12	1.13
S-2	215.8	214.5	415	413	1.05	1.08	1.17	1.20
S-3	219	218.9	430	430	1	1	1	1

$$SLR = \left(\frac{\epsilon_{v1}}{\epsilon_{v2}} \right)^{4.5337} \tag{6}$$

where ϵ_{v1} and ϵ_{v2} are a maximum vertical compressive strain at the top of the subgrade for the control section (S-3) and geocell reinforced-fly ash (S-1 & S-2) section, respectively. The SLR of pavement against fatigue failure is calculated by Eq. (7),

$$SLR = \left(\frac{\epsilon_{t1}}{\epsilon_{t2}} \right)^{3.89} \tag{7}$$

where ϵ_{t1} and ϵ_{t2} are a maximum horizontal tensile strain at the bottom of the bituminous layer for the control section (S-3) and geocell-reinforced fly ash (S-1 & S-2) section, respectively, the SLR values are measured against

the granular control section (S-3) for 40 and 55 kN FWD loading.

The SLR value for both geocell reinforced-fly ash sections (S-1 & S-2) against the granular control section (S-3) is more than 1 for both rutting and fatigue failure, which confirms the suitability of geocell-reinforced fly ash in the subbase layer. The higher SLR values are obtained against higher FWD loading (55 kN), which indicates the improved performance of the ‘geocell reinforced-fly ash’ test section under heavy trafficking.

Conclusions

The field performance of ‘geocell-reinforced fly ash’ as a subbase layer was evaluated during construction by a light weight deflectometer (LWD) test over the base course

and after construction by a falling weight deflectometer (FWD) test over the surface course. During construction, a positive effect of geocell-reinforced fly ash was observed on composite in-situ modulus and quantified in terms of composite modulus improvement factor (CMIF). After construction, a positive impact of geocell-reinforced fly ash was observed on the subbase layer's average elastic modulus and quantified in terms of modular ratio (MR). Furthermore, finite element analysis was carried out to determine service life ratio (SLR) against fatigue and rutting failure. The following conclusions can be drawn:

- LWD successfully captured the benefits of geocell-reinforced fly ash through in-situ composite modulus and confirms the suitability of the same as a subbase layer in the pavement.
- The CMIF value for the 100-mm-high geocell-reinforced fly ash section was 1.19, and the 150 mm high geocell-reinforced fly ash section was 1.39 against the granular control section. The higher value of the CMIF confirms the suitability of geocell-reinforced fly ash in the subbase layer.
- The MR values were calculated for both the FWD load (44 kN and 55 kN) and for both the testing periods (August 2019 and February 2021). In each FWD testing, the MR value of the geocell-reinforced fly ash layer was greater than 1; it shows the suitability of 'geocell-reinforced fly ash' as a subbase layer in the pavement. The MR value varies between 1.16 and 1.22 for the 100-mm-high geocell-reinforced fly ash layer. The highest MR value of 1.30 was observed for the 150-mm-high geocell-reinforced fly ash layer during the second FWD testing with 55 kN loading.
- The SLR value for both geocell-reinforced fly ash sections (S-1 & S-2) against the granular control section (S-3) is more than 1 for both rutting and fatigue failure, which further confirms the suitability of geocell-reinforced fly ash in the subbase layer.
- The higher SLR values were obtained against higher FWD loading (55 kN), which indicates the improved performance of the 'geocell-reinforced fly ash' test section under heavy trafficking. The SLR value for fatigue was increased from 1.06 to 1.08 with an increase in geocell height from 100 to 150 mm for higher FWD loading (55 kN). Similarly, the SLR value for rutting was increased from 1.13 to 1.20 with an increase in geocell height from 100 to 150 mm for higher FWD loading (55 kN).

Acknowledgements The authors acknowledge the support of the Roads and Buildings Department (Surat, India) during the construction of the test section and field testing. The authors are also thankful to Maccaferri (India) for providing geocell material.

Author contributions Conceptualization: SP, JTS; methodology: RRD, SP; formal analysis and investigation: RRD; resources: SP, JTS; software: RRD; writing—original draft preparation: RRD, SP; supervision: SP, JTS.

Funding The authors have no relevant financial or non-financial interests to disclose.

Declarations

Conflict of interest The authors have no competing interests to declare that are relevant to the content of this article.

References

1. Patel D, Kumar R, Chauhan KA, Patel S (2019) Experimental and modeling studies of resilient modulus and permanent strain of stabilized fly ash. *J Mater Civil Eng* 31(8):06019005. [https://doi.org/10.1061/\(asce\)mt.1943-5533.0002798](https://doi.org/10.1061/(asce)mt.1943-5533.0002798)
2. IRC SP 20 (2002) Rural roads manual. Indian Road Congress, Special Publication, New Delhi
3. Zhou H, Wen X (2008) Model studies on geogrid- or geocell-reinforced sand cushion on soft soil. *Geotext Geomembr* 26(3):231–238. <https://doi.org/10.1016/j.geotextmem.2007.10.002>
4. Han J, Pokharel SK, Yang X, Manandhar C, Leshchinsky D, Halahmi I, Parsons RL (2011) Performance of geocell-reinforced RAP bases over weak subgrade under full-scale moving wheel loads. *J Mater Civ Eng ASCE* 23(11):1525–1534. [https://doi.org/10.1061/\(ASCE\)MT.1943-5533.0000286](https://doi.org/10.1061/(ASCE)MT.1943-5533.0000286)
5. Madhavi Latha G, Rajagopal K (2007) Parametric finite element analyses of geocell-supported embankments. *Can Geotech J* 44(8):917–927. <https://doi.org/10.1139/t07-039>
6. Hegde AM, Sitharam TG (2015) Effect of infill materials on the performance of geocell reinforced soft clay beds. *Geomech Geoeng* 10(3):163–173. <https://doi.org/10.1080/17486025.2014.921334>
7. Kief O, Schary Y, Pokharel SK (2015) High-modulus geocells for sustainable highway infrastructure. *Indian Geotech J* 45(4):389–400. <https://doi.org/10.1007/s40098-014-0129-z>
8. Dutta S, Mandal JN (2016) Model studies on geocell-reinforced fly ash bed overlying soft clay. *J Mater Civ Eng ASCE* 28(2):1–13. [https://doi.org/10.1061/\(ASCE\)MT.1943-5533.0001356](https://doi.org/10.1061/(ASCE)MT.1943-5533.0001356)
9. Kumawat NK, Tiwari SK (2017) Bearing capacity of square footing on geocell reinforced fly ash beds. *Mater Today: Proc* 4(9):10570–10580. <https://doi.org/10.1016/j.matpr.2017.06.422>
10. Edil TB, Benson CH, Mengelt M (2006) Resilient modulus and plastic deformation of soil confined in a geocell. *Geosynth Int* 13(5):195–205. <https://doi.org/10.1680/gein.2006.13.5.195>
11. Yang X, Han J, Pokharel SK, Manandhar C, Parsons RL, Leshchinsky D, Halahmi I (2012) Accelerated pavement testing of unpaved roads with geocell-reinforced sand bases. *Geotext Geomembr* 32:95–103. <https://doi.org/10.1016/j.geotextmem.2011.10.004>
12. Al-Qadi I, Hughes J (2000) Field evaluation of geocell use in flexible pavements. *Transp Res Rec* 1709:26–35. <https://doi.org/10.3141/1709-04>
13. Umashankar B, Hariprasad C, Kumar GT (2016) Compaction quality control of pavement layers using LWD. *J Mater Civ Eng ASCE* 28(2):1–9. [https://doi.org/10.1061/\(ASCE\)MT.1943-5533.0001379](https://doi.org/10.1061/(ASCE)MT.1943-5533.0001379)
14. Kumar R, Kumar VA, Guzzarlapudi SD (2017) Stiffness-based quality control evaluation of modified subgrade soil using

- lightweight deflectometer. *J Mater Civ Eng ASCE* 29(9):1–9. [https://doi.org/10.1061/\(ASCE\)MT.1943-5533.0001958](https://doi.org/10.1061/(ASCE)MT.1943-5533.0001958)
15. Deshmukh RR, Patel S, Shahu JT (2021) Field assessment of improvement in composite modulus of geosynthetic-reinforced pavements. *Geosynth Int ICE* 28(6):624–633. <https://doi.org/10.1680/jgein.21.00018>
 16. ASTM D248–17 (2017) Standard Practice for Classification of Soils for Engineering Purposes (Unified Soil Classification System), American Society for Testing and Materials, West Conshohocken, PA, USA.
 17. MoRTH (2013) Specifications for road and bridge work. Ministry of Road Transport and Highway (MoRTH) 5th edn. Indian Roads Congress, New Delhi
 18. IS 2720 (Part 7) (1980) Determination of water content-dry density relation using light compaction. Bureau of Indian Standards, New Delhi
 19. IS 2720 (Part 16) (1987) Laboratory determination of CBR. Bureau of Indian Standards, New Delhi
 20. ASTM C618–17 (2017) Standard specification for coal fly ash and raw or calcined natural pozzolan for use as a mineral admixture in concrete, American Society for Testing and Materials, West Conshohocken, PA, USA.
 21. Patel S, Shahu JT (2018) Comparison of industrial waste mixtures for use in subbase course of flexible pavements. *J Mater Civil Eng* 30(7):04018124. [https://doi.org/10.1061/\(asce\)mt.1943-5533.0002320](https://doi.org/10.1061/(asce)mt.1943-5533.0002320)
 22. IRC 37 (2012) Tentative guideline for the design of flexible pavements. Indian Road Congress, New Delhi
 23. IS 2720 (Part 28) (1974) Determination of dry density of soils in-place, by the sand replacement method. Bureau of Indian Standards, New Delhi
 24. ASTM D6951/D6951M-18 (2018) Standard Test Method for Use of the Dynamic Cone Penetrometer in Shallow Pavement Applications, American Society for Testing and Materials, West Conshohocken, PA, USA.
 25. ASTM E2583–07 (2007) Standard Test Method for Measuring Deflections with a Light Weight Deflectometer (LWD). American Society for Testing and Materials, West Conshohocken, PA, USA.
 26. Fleming PR, Frost MW, Lambert JP (2007) Review of the lightweight deflectometer (Lwd) for routine in-situ assessment of pavement material stiffness. *Transp Res Rec* 2004(1):80–87. <https://doi.org/10.3141/2004-09>
 27. IRC 115 (2014) Guidelines for structural evaluation and strengthening of flexible road pavements using falling weight deflectometer (FWD) technique. Indian Road Congress, New Delhi
 28. Shahu JT, Patel S, Senapati A (2013) Engineering properties of copper slag-fly ash–dolime mix and its utilization in the base course of flexible pavements. *J Mater Civil Eng*. 25(12):1871–1879. [https://doi.org/10.1061/\(asce\)mt.1943-5533.0000756](https://doi.org/10.1061/(asce)mt.1943-5533.0000756)
 29. Chaudhary PM, Chaudhary PB, Desai BH, Deshmukh R (2021) Design and performance of highway pavement reinforced with geosynthetic. In: Patel S, Solanki CH, Reddy KR, Shukla SK (eds) *Proceedings of the Indian Geotechnical Conference 2019*, vol 137. Springer, Singapore. https://doi.org/10.1007/978-981-33-6466-0_33 (**Lecture Notes in Civil Engineering**)

Publisher's Note Springer Nature remains neutral with regard to jurisdictional claims in published maps and institutional affiliations.